symmetry

MDPI

Article

Roles of Hydrogen, Halogen Bonding and Aromatic Stacking in a Series of Isophthalamides

Islam Ali Osman [1], Vickie McKee [2], Christian Jelsch [3] and John F. Gallagher [1,*]

[1] School of Chemical Sciences, Dublin City University, D09 E432 Dublin, Ireland
[2] Department of Physics, Chemistry and Pharmacy, University of Southern Denmark, Campusvej 55, 5230 Odense M, Denmark
[3] CRM2, CNRS UMR 7036, Faculté des Sciences et Technologies, Université de Lorraine, 54000 Nancy, France
* Correspondence: john.gallagher@dcu.ie

Simple Summary: Crystal and modelled structures of five N^1,N^3-di(5-**X**-pyridin-2-yl)isophthalamides (**X** = H, F to I) as (**X-DIP**) are reported. The roles that their molecular conformations and interactions play in solid-state aggregation are assessed. **Cl-DIP** (Z' = 3) exhibits both ***syn*/*anti*** and ***anti*/*anti*** molecular conformations in 2:1 ratio. The hydrogen bonding hierarchy and sheet formation in **Br-DIP** induces the formation of a bromine-rich environment manifesting as a 'wall of bromine atoms' at the sheet interfaces. The hydrate in **I-DIP**•$^1/_2$(H_2O) forms a rare synthon.

Abstract: The synthesis and spectroscopic characterisation of six bis(5-**X**-pyridine-2-yl)isophthalamides (**X** = H, F, Br, Cl, I, NO_2) are reported, together with five crystal structure analyses (for **X** = H, F to I). The isophthalamides span a range of conformations as ***syn*/*anti*** (**H-DIP**; **I-DIP**), ***anti*/*anti***- (**F-DIP**; **Br-DIP**) and with both present in ratio 2:1 in **Cl-DIP**. The essentially isostructural **F-DIP** and **Br-DIP** molecules (using strong amide ... amide interactions) aggregate into 2D molecular sheets that align with either F/H or Br atoms at the sheet surfaces (interfaces), respectively. Sheets are linked by weak C-H···F contacts in **F-DIP** and by Br···Br halogen bonding interactions as a 'wall of bromines' at the Br atom rich interfaces in **Br-DIP**. **Cl-DIP** is an unusual crystal structure incorporating both ***syn*/*anti*** and ***anti*/*anti*** molecular conformations in the asymmetric unit (Z' = 3). The **I-DIP**•$^1/_2$(H_2O) hemihydrate structure has a water molecule residing on a twofold axis between two **I-DIP**s and has hydrogen and N···I (N_c = 0.88) halogen bonding. The hydrate is central to an unusual synthon and involved in six hydrogen bonding interactions/contacts. Contact enrichment analysis on the Hirshfeld surface demonstrates that **F-DIP**, **Cl-DIP** and **Br-DIP** have especially over-represented halogen···halogen interactions. With the **F-DIP**, **Cl-DIP** and **Br-DIP** molecules having an elongated skeleton, the formation of layers of halogen atoms in planes perpendicular to the long unit cell axis occurs in the crystal packings. All six **DIP**s were analysed by ab initio calculations and conformational analysis; comparisons are made between their minimized structures and the five crystal structures. In addition, physicochemical properties are compared and assessed.

Keywords: aggregate; aromatic ring stacking; crystal structure; conformational analysis; halogen bonding; hydrogen bonding; interactions

Citation: Osman, I.A.; McKee, V.; Jelsch, C.; Gallagher, J.F. Roles of Hydrogen, Halogen Bonding and Aromatic Stacking in a Series of Isophthalamides. *Symmetry* **2023**, *15*, 738. https://doi.org/10.3390/sym15030738

Academic Editor: Anatoly S. Buchelnikov

Received: 31 January 2023
Revised: 23 February 2023
Accepted: 2 March 2023
Published: 16 March 2023

1. Introduction

The structural chemistry of potentially useful organic ligands for applications in a range of scientific areas, such as coordination chemistry, bioinorganic, medicinal chemistry and drug development, continues unabated [1–4]. At the heart of the many and varied classes of organic ligands lies the benzamide/carboxamide group of compounds and their derivatives such as isophthalamides [5–7]. These and closely related compounds have been developed over the past two decades and especially in the drive to acquire a deeper and more fundamental knowledge in foldamer chemistry and host•guest science [8–10].

In structural science, the hierarchy of interactions has been the subject of much discussion in the past few decades with considerable effort in identifying key synthons in molecular aggregation and their ranking in crystal structure formation [11–15]. The effects of various interactions, for example in competition/interplay between hydrogen and halogen bonding, have been assessed [11–15]. Benzamides and their foldamer derivatives have proven to be convenient compounds to study in order to gain a greater insight into intermolecular interactions, conformational analyses and helical structures in foldamers [8–10].

Benzamides and related ligands such as carboxamides and carbamates have proven important as ligands in coordination chemistry, and especially those incorporating pyridine or related heteroaromatic groups [16–23]. Herein, we report the synthesis and spectroscopic characterisation of six N^1,N^3-di(5-X-pyridin-2-yl)isophthalamides or **X-DIP**s in a series (X = H, F, Cl, Br, I, NO_2; Scheme 1). All crystal structures, except **X** = NO_2, were determined. Comparisons are made between the solid-state structures and modelled structures as obtained from ab initio calculations [17–19]. A variety of conformations are obtained and in the **Cl-DIP** structure two distinct conformations are observed in a Z' = 3 structure. Isophthalamides such as these are proving to be important compounds in terms of their structural chemistry as well as their utilisation in metal coordination chemistry, where the halogen substitution can influence the overall metal complex properties [5–7,23].

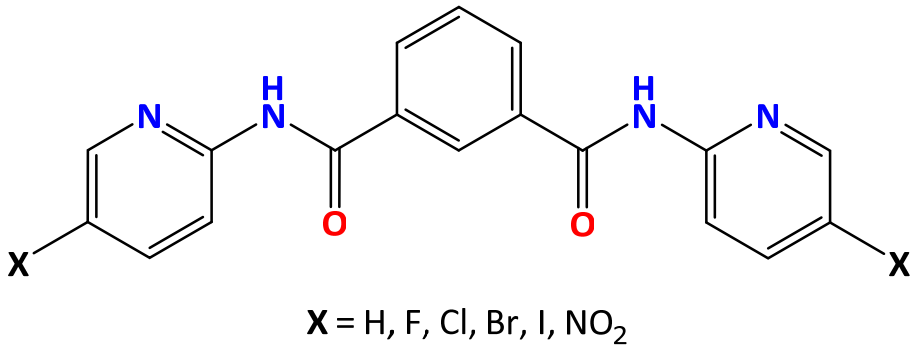

Scheme 1. The N^1,N^3-bis(5-**X**-pyridin-2-yl)isophthalamides (**X** = H, F to I, NO_2) or **X-DIPs** as depicted in the ***anti*/*anti*** conformation (with respect to the amide groups).

2. Experimental

2.1. Materials and Characterisation

The materials used, IR and NMR spectra, crystallographic methods, programs and equipment are as documented in previous papers. Further spectroscopic and analytical details are provided in the **ESI** (**part I**) [17,24].

2.2. Synthetic Procedures (1 and 2)

Two procedures were used in the isophthalamide synthesis (as described for 2-aminopyridine). Both involved standard condensation procedures and differed by using isophthalic acid (route 1) and isophthaloyl dichloride (route 2) as starting materials and the subsequent workup (Scheme 2) [25].

In route 1 (Scheme 2), the synthesis of N^1,N^3-di(pyridine-2-yl)isophthalamide involves the condensation reaction of isophthalic acid with 2-aminopyridine in pyridine solvent using triphenylphosphite [$P(OPh)_3$] at ~110 °C. Thus, isophthalic acid (2.08 g, 12.5 mmol), 2-aminopyridine (3.54 g, 37.5 mmol) with 50 mL pyridine and a magnetic stirrer were placed in a 100 mL round-bottom flask (RBF). This mixture in an oil bath, equipped with a reflux condenser, was warmed with stirring for 15–20 min to 40 °C until both chemicals dissolved. Triphenylphosphite (9.9 mL, 37.5 mmol) was added through the condenser (using a 10 mL pipette) and the mixture was heated under reflux conditions at 110 °C for 12 h. The reaction flask and contents were cooled to room temperature. The pyridine solvent was removed by evaporation on a rotary evaporator equipped with a high vacuum pump (80–90 °C/20 mbar). The resulting viscous red-brown oil was dissolved in 150 mL of

dichloromethane (CH_2Cl_2), and the product was extracted twice with 150 mL 1:1 (*v*/*v*) of dilute HCl. Each of the acidic aqueous extracts was transferred into a 500 mL Erlenmeyer flask on an ice bath. The pH of acidic solution was slowly neutralised with a concentrated aqueous solution of NaOH and solid Na_2CO_3 to a pH of 7–8. The mixture was cooled slowly to enhance the formation of a white precipitate. The white solid was filtered on a Buchner's funnel and washed thoroughly with water to remove traces of pyridine and the solid was left to dry overnight. The product was dissolved in 150–200 mL of CH_2Cl_2 (DCM) and the solution washed with an aqueous solution of $NaHCO_3$ and Na_2CO_3. The organic layer was dried with $MgSO_4$ and a small amount of charcoal added. The solution was double-filtered, and the product recovered after solvent evaporation.

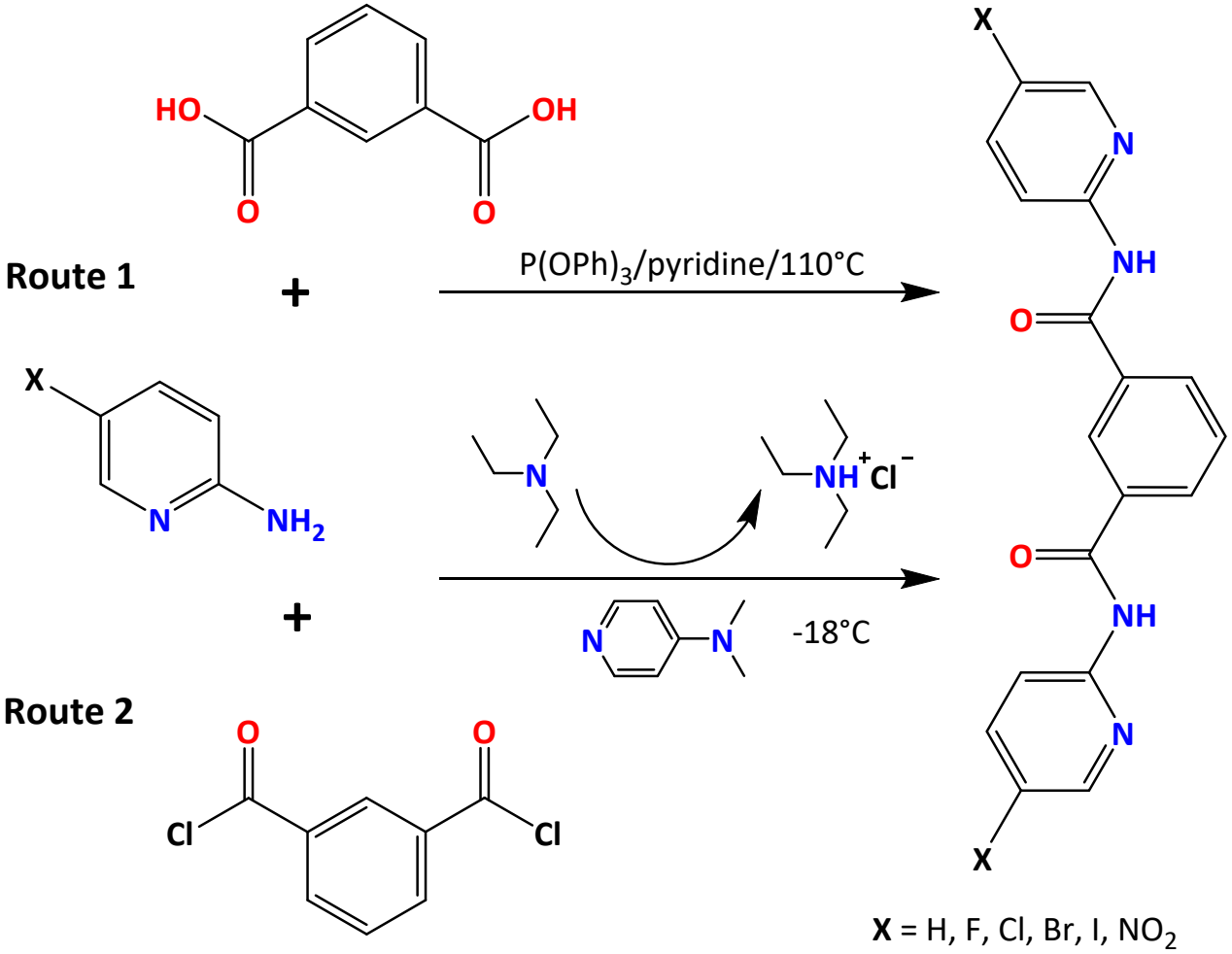

Scheme 2. Isophthalic acid (1) and isophthaloyl dichloride (2) synthetic routes [25].

In the second route (Scheme 2), the reaction of isophthaloyl dichloride with 2-aminopyridine in the presence of triethylamine (Et_3N) and 4-(dimethylamino)pyridine (DMAP) was performed at −18 °C. Isophthaloyl dichloride (2.03 g, 10 mM) and 2-aminopyridine (1.88 g, 20 mM) were suspended in 50 mL of dry DCM and poured into a flask and placed in an ice bath (−18 °C to 0 °C). Then, Et_3N (5 mL, 20mM) was added dropwise over 10 min and the reaction mixture stirred for 4 hrs. The reaction solution was filtered under vacuum, the filtrate powder was collected and the solution was removed by a rotary evaporator. The resulting residue was dissolved in 200 mL of DCM and the solution was washed with aqueous solutions of $NaHCO_3$ and Na_2CO_3. The organic layer was dried with $MgSO_4$ and a small amount of charcoal was added, then filtered. Finally, the product was recovered after evaporation of solvent.

Route 1 was used to synthesise **H-DIP**. For **F-DIP**, **Cl-DIP**, **Br-DIP**, **I-DIP** and **NO_2-DIP**, the extraction step was the last step; further re-purification had no significant effect on product purity. **H-DIP** and **F-DIP** were obtained in a reasonably pure grade because their starting materials had good water solubility. However, both **Cl-DIP** and **Br-DIP** syntheses gave a mixture of starting materials and products which were insoluble in water. In the **Cl-DIP** and **Br-DIP** extraction, the first extraction from DCM by aqueous HCl gave a high quantity of the product and starting materials, and the second extraction gave a low yield of pure product. These two extractions were not mixed. For **Br-DIP**, the amount of unreacted starting material was much higher than the desired product. Therefore, the mixture was reused in a fresh reaction and heated at reflux conditions over 48 h. This gave a higher product yield than starting material although a mixture was still obtained. Liquid chromatography was performed to purify both **Cl-DIP** and **Br-DIP**. For **I-DIP**, a low yield of pure product was obtained by this route. However, the **NO_2-DIP** synthesis did not work despite the reaction being heated at reflux temperatures overnight. Although the pyridine solvent colour became very deep red in colour, the extracted product only contained starting material.

Synthetic route 2 was developed to overcome the low reactivity in route 1 that failed to produce **NO_2-DIP**. Isophthaloyl dichloride was reactive, and the reaction temperature was lowered to −18 °C with Et_3N added dropwise to control the reaction rate. The **NO_2-DIP** purification process was not sufficient to obtain a pure product (as determined by TLC and NMR) by this approach. Therefore, column chromatography was used to purify the final **NO_2-DIP** product using a mixture of DCM:ethyl acetate (95:5) as a mobile phase.

F-DIP gave the desired product with a high yield of 98%. The product was filtered directly from the reaction mixture with a high purity. In addition, the purification of **H-DIP**, **Cl-DIP** and **Br-DIP** by washing with Na_2CO_3 was sufficient to obtain significantly high yields of pure products by this route when compared to route 1 [25].

Single crystal X-ray data collections, processing and refinements for the five **X-DIPs** (Scheme 1) are as detailed previously [17,24,26]. Data were collected using Mo and Cu radiation for **Cl-DIP**, but only Cu data are discussed herein. The **H-DIP** and **I-DIP**•$^1/_2(H_2O)$ data were collected using an XtaLAB Synergy, Dualflex, ATLAS2 at 100(1) K [24] and the **F-DIP**, **Cl-DIP** and **Br-DIP** data at 294(1) K on a Xcalibur Sapphire 3, Gemini diffractometer [17]. Selected crystallographic and structural data are in Tables 1 and 2 and full details are in Figures S1–S9 and Tables S1–S3 in the **ESI** (**Part II**). Molecular and crystal structure diagrams (Figures 1–5) are standard [27,28]. Computational calculations and methods are as described (**ESI Part I**) [19,29–31]. Crystal structure comparisons were performed with Conquest 2022.1.0 and CSD 2022 version (5.43 + 4 updates) [32].

Table 1. Selected crystallographic data for **X-DIP**s (full details are listed; **ESI Part II**).

Crystal Structure	Crystal System: Space Group	Z'	Volume (Å^3)	R, wR_2 R-Factors, GoF
H-DIP	Triclinic, $P\,\bar{1}$ (No. 2)	1	713.43 (4)	0.031, 0.078, 1.030
F-DIP	Monoclinic, $P2_1/c$ (No. 14)	1	1559.71 (8)	0.045, 0.111, 1.026
Cl-DIP	Triclinic, $P\,\bar{1}$ (No. 2)	3	2553.5 (3)	0.062, 0.162, 1.075
Br-DIP	Monoclinic, $C2/c$ (No. 15)	1	3509.3 (6)	0.078, 0.205, 1.045
I-DIP•$^1/_2(H_2O)$	Monoclinic, $P2/c$ (No. 13)	1	1814.49 (5)	0.023, 0.056, 1.060

Footnote: R-factors defined as $R[F^2 > 2\sigma(F^2)]$, $wR(F^2)$ [26]. GoF: goodness of fit.

Table 2. Salient structural features of the five **X-DIP**s: angle between planes (°) and H-bond donor· · · acceptor distances (Å).

Structure	C_6/C_5N	C_6/Amide	C_5N/Amide	N· · ·N/O #	Primary H-Bond
H-DIP	68.17 (3) 5.65 (7)	49.60 (4) 19.49 (6)	15.04 (15) 14.10 (6)	3.1252 (13) 3.3425 (13)	amide· · · amide amide· · · pyridine
F-DIP	47.20 (4) 14.20 (6)	45.69 (4) 10.47 (7)	3.22 (7) 3.97 (7)	3.3129 (19) 3.2605 (16)	amide· · · amide amide· · · pyridine
Cl-DIP (in sequence for molecules A, B, C)	11.6 (3) 15.7 (3), 10.3 (3) 24.5 (2), 9.3 (3) 10.2 (3)	30.3 (2) 31.6 (2), 29.3 (2) 21.8 (2), 33.5 (2) 19.4 (2)	26.6 (2) 17.3 (3), 20.7 (3) 3.0 (3), 26.9 (2) 28.9 (2)	2.924 (4) 3.029 (5), 2.973 (4) 3.289 (4), 2.865 (4) 3.078 (4)	amide· · · amide
Br-DIP	36.4 (2) 46.6 (2)	38.8 (2) 1.5 (4)	2.6 (3) 47.8 (2)	3.186 (8) 2.999 (8)	amide· · · amide amide· · · pyridine
I-DIP•1/2(H_2O)	4.6 (2) 19.21 (15)	28.8 (3) 9.0 (6)	24.2 (3) 10.2 (5)	2.897 (4) 2.931 (3) 2.833 (3)	amide· · · H_2O (pyridine)N· · · I-C

Footnote: C_6 is the isophthaloyl ring; C_5N represents the terminal pyridine rings. The amides are represented as the adjoining five atom C-C(=O)NC plane. The # refers to the 'Primary hydrogen bonding· · · pyridine'. Primary hydrogen bonding; usually as either amide· · · amide or amide· · · pyridine.

3. Methods

Fingerprint plots of contacts on the Hirshfeld surface around the molecules were computed with CrystalExplorer17 [33] (**ESI**). The Hirshfeld surface contact statistics and enrichment ratios were acquired using MoProViewer [34]. In the latter case, the hydrophobic hydrogen atom H_C attached to a carbon atom is distinguished from H_P the more polar and charged the $H_{O/N}$ atoms attached to N or O are. Enrichments of hydrophobic contacts and of H bonds are depicted in Figure 6. The contact types on the 3 independent **Cl-DIP** molecules were averaged as the contacts C_{XY} between chemical species X and Y and showed globally a 97% correlation (Figure S8). In the case of the iodinated **I-DIP**•1/2(H_2O) structure with half a water molecule (hemi-hydrate) in the asymmetric unit, the Hirshfeld surface was computed around an ensemble of one water and two **I-DIP**•1/2(H_2O) molecules; molecules not in contact with each other were selected in the crystal packing in order to obtain integral Hirshfeld surfaces about all three entities.

4. Results and Discussion

4.1. Crystal and Molecular Structural Analysis of H-DIP

The **X-DIP** molecules contain two amides [O=CN(H)] and two pyridine rings per molecule and therefore each **X-DIP** possesses two donor N-Hs and four acceptors (2 × O=C, 2 × $N_{pyridine}$) (Figure 1). The donor:acceptor mismatch is usually compensated by C-H donors pairing with the free O or N in the **X-DIP** crystal structures.

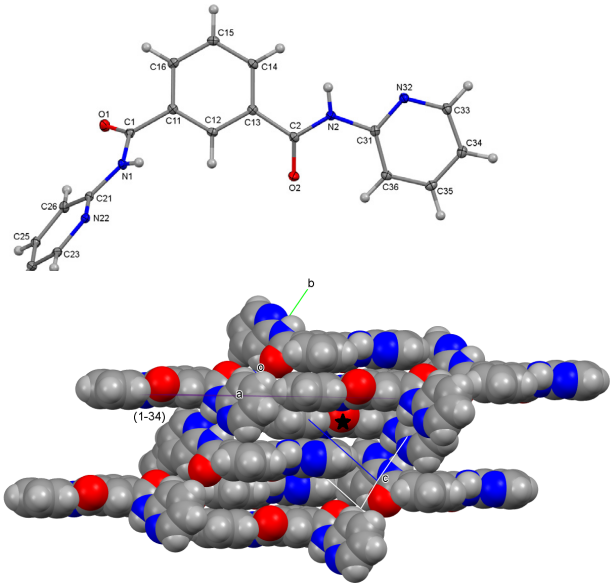

Figure 1. An ORTEP view of **H-DIP** and the intermolecular interactions with cyclic N-H···N, N-H···O=C chains (★), aromatic stacking and C-H···π(arene) contacts.

4.2. H-DIP: Short C-H···π(Arene) Contacts and Tight Ring···Ring Stacking

The **H-DIP** crystal structure in space group $P\,\bar{1}$ (No. 2) refines to R = 3.1% without issues [26]. **H-DIP** molecules adopt the ***syn*/*anti*** molecular conformation (Figure 1) as noted by Malone and co-workers in **PULHUZ** [5,32]. The **H-DIP** structure exhibits a range of intermolecular interactions and contacts especially involving the two amide and the two pyridines yielding amide···pyridine N1-H1···N22^{i} hydrogen bonds with centrosymmetric rings. **H-DIP** also forms chains of amide···amide intermolecular interactions as N2-H2···O2=C2^{ii} H bonds with symmetry codes (*i*, *ii* in Table S2, **ESI Part II**). The N1-H1···N22^{i} interactions form cyclic $R^2_2(8)$ hydrogen-bonded rings augmented by C23-H23···π(arene)^{i} contacts (H23···Cg^{i} = 2.63 Å, 156°; [2.51 Å, 155° with normalized C-H]) and with N2···O2^{ii} generating 1D columns along the *a*-axis direction [17]. With two amides (N1, N2, O1, O2) and two pyridine N22, N32 atoms per **H-DIP** (underline for amide···amide or pyridine···pyridine interactions), the amide carbonyl O1 and pyridine N32 only participate in weaker, cyclic C25-H25···(O1=C1)^{iii} as $R^2_2(14)$ rings and C15-H15···N32^{iv} interactions as $R^2_2(16)$ rings (Table S2). This results in 1D columns linking via C25-H25···O1^{iii} and C15-H15···N32^{iv} interactions and aromatic stacking.

H-DIP molecules aggregate as pairs through aromatic stacking about inversion centres (Figure 1); this involves two approximately co-planar aromatic rings having a pyridine and a benzene ring mutually oriented at 5.65(7)°. Pairs of **H-DIP** molecules interact via parallel offset stacking involving pyridine rings resulting in offset stacked columns in the crystal structure and with aromatic rings parallel with the (1 $\bar{3}$4) plane. The closest stacking contact is the pyridine ring C36···C36^{xiv} tight contact distance of 3.2864(16) Å for inversion-symmetry-related C36 atoms (Table S2). The short C-H···π(arene) contact involving C23-H23···π(C11, . . . ,C16)^{i} that augments the N1-H1···N22^{i} cyclic interaction has a short H23···(Cg1 ring centroid)^{i} = 2.63 Å distance and is similar in geometry to those in the tightly interacting dimers of **Moo** where C-H···π(arene) contacts form in tandem with strong N-H···N hydrogen bonding [17].

4.3. F-DIP

F-DIP was grown from a CH_2Cl_2/acetone mixture and adopts the ***anti*/*anti*** molecular conformation in space group $P2_1/c$ (No. 14) (Figure 2). The central molecular C_6 ring and a fluoropyridine ring (F34) are mutually oriented close to planarity at an interplanar angle of 14.20(6)°, but at angles of 47.20(4)° and 48.55(4)° to the F24 fluoropyridine ring,

respectively. Both amido groups lie close to planarity with the fluoropyridine rings to which they are attached, at 3.22(7)° and 3.97(7)°.

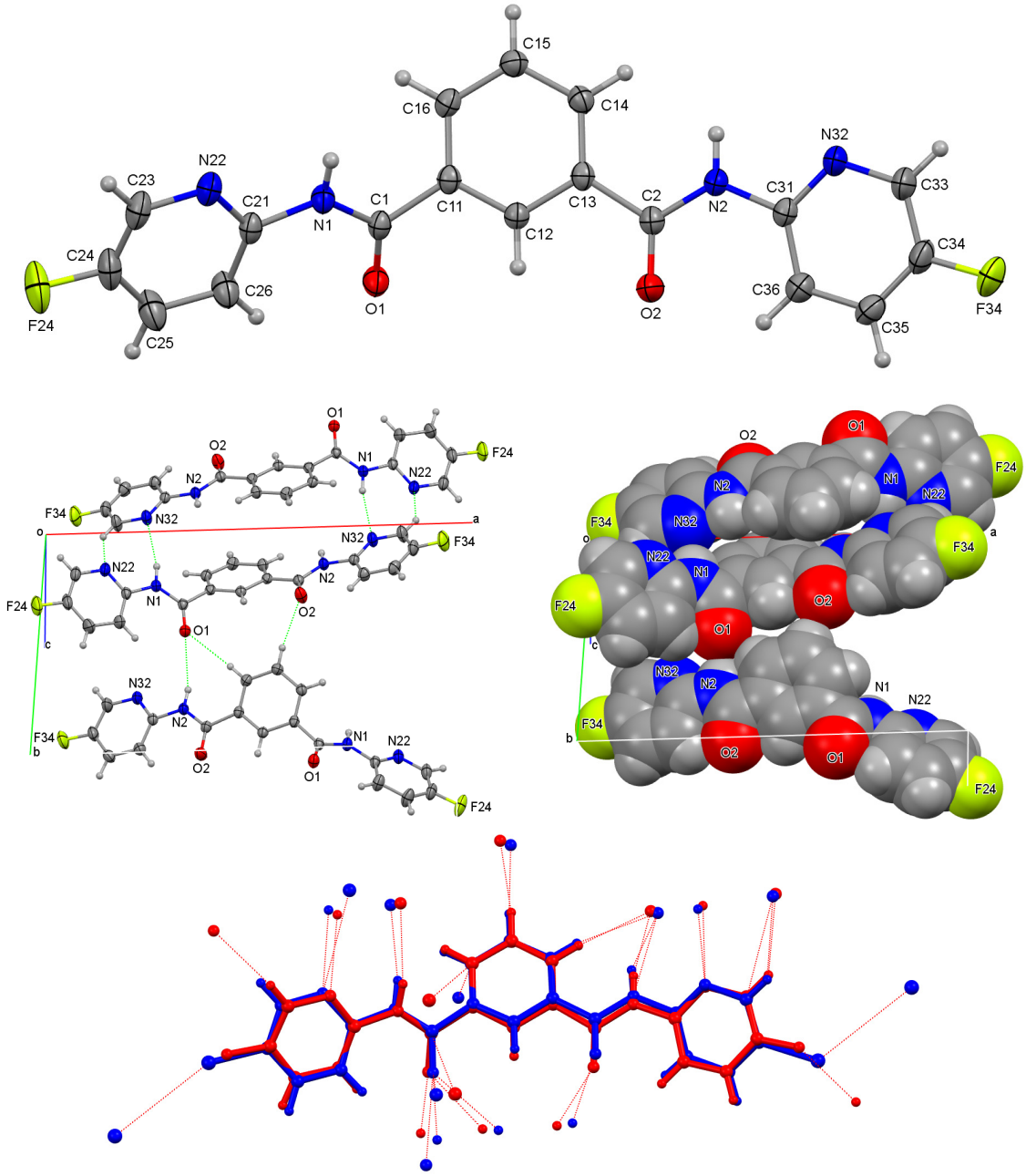

Figure 2. An ORTEP view of **F-DIP** (top) with two views of the main intermolecular interactions; an overlay of the **F-DIP** (in $P2_1/c$) and **Br-DIP** structures (in $C2/c$) with interactions and close contacts.

F-DIP aggregates through the formation of tight hydrogen-bonded dimers. This arises via N1-H1$\cdots$N32^{v} hydrogen bonding about inversion centres, graph set $R^2_2(20)$, with N1$\cdots$N32^{v} = 3.3129(19) Å and in tandem with the reciprocal (C33-H33)$^{v}\cdots$N22 = 3.269(2) Å, graph set = $R^2_2(7)$ and offset amide$\cdots$aromatic ring stacking. The hydrogen-bonded dimers are linked by the second amide N-H as the N2-H2$\cdots$O1=C1^{vi} = 3.2605(16) Å interaction (two per dimer, assisted by C14-H14 as $R^1_2(7)$). The O2=C2 is involved in weaker C15-H15$\cdots$(O2=C2)^{vi} interactions, though from the same molecule. The H$\cdots$N/O distances are within the range 2.36 to 2.52 Å (with D$\cdots$A is 3.2605(16) to 3.3936(17) Å, with angles from 138° to 174°). The hydrogen-bonded aggregate forms one-molecule-

wide molecular sheets parallel with (100) and linked by C23-H23$\cdots$F34^{viii} intermolecular contacts (with H23$\cdots$F34^{viii} = 2.61 Å, C-H$\cdots$F of 126°) spanning the sheets (Figure S3b). **F-DIP** has all of its strong donors/acceptors engaged in intermolecular hydrogen bonding which is augmented by both intramolecular and intermolecular C-H$\cdots$O contacts.

In contrast to **F-DIP**, the **TOYQIJ** molecular structure [32,35] (differing only from **F-DIP** by the $_{ipso}$C-H C12-H12 replaced by N), adopts a ***syn*/*syn*** conformation. The conformational stability of **TOYQIJ** is enhanced by two intramolecular N-H$\cdots$N$_{\text{pyridine}}$ interactions involving the central pyridine N atom in preference to forming either of the ***syn*/*anti*** (as in **H-DIP**) or ***anti*/*anti*** conformations (in **F-DIP**) as favored by having the C12-H12 moiety. This is a recurring feature in the **X-DIP** molecular systems in comparison to their pyridine relatives.

4.4. Cl-DIP: A Crystal Structure (Z′ = 3) with Two Different Conformations

Cl-DIP (as grown from ethyl acetate) crystallises with three independent molecules in the asymmetric unit (Z' = 3) in space group $P\,\bar{1}$ (No. 2). **Cl-DIP** is a rare example of a crystal structure with two distinct conformations (in ratio 1:2). Molecule A adopts the ***anti*/*anti*** molecular conformation and is similar to **F-DIP**, whereas molecules B and C have the ***syn*/*anti*** conformation and are more comparable in structure to **H-DIP** (Figure 3). The molecular conformations clearly differ as exemplified by the *para* [Cl1 ... C15 ... Cl2]$_{A/B/C}$ angles of 125.06(4)° (molecule A), 104.75(4)° (B) and 110.41(4)° (C) with the two smaller angles for the ***syn*/*anti*** conformations. The aromatic rings and amide groups in **Cl-DIP** do not twist much from co-planarity and the largest twist is 33.5(2)° for the two flanking fluoropyridine rings in molecule B, with corresponding data for molecules A and C being 8.5(3)° and 5.8(3)°.

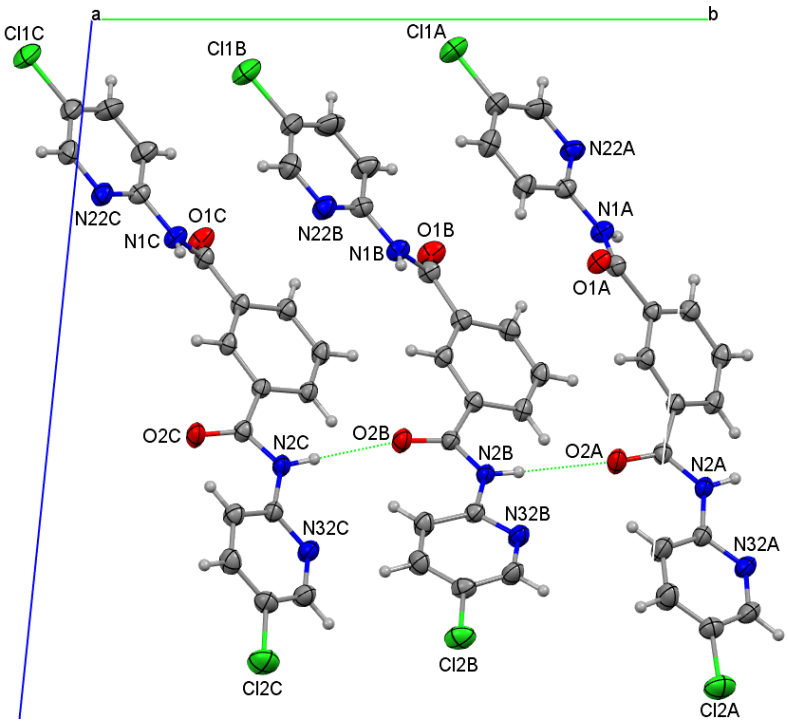

Figure 3. *Cont.*

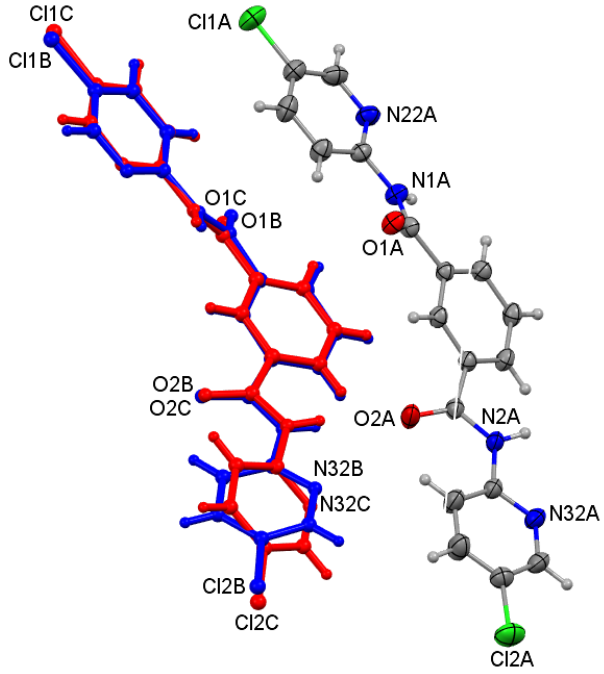

Figure 3. Asymmetric unit of **Cl-DIP** and overlay of molecule A (ORTEP) with molecules B and C.

The aggregation is of interest in that all six amides in molecules A to C are involved in N-H···O=C interactions. There are no strong N-H···$N_{pyridine}$ hydrogen bonding interactions as the amide donors/acceptors are all utilised in strong amide···amide intermolecular interactions. The molecules aggregate (using one of the two amide groups per molecule) forming individual chains of (A ... A ...)$_n$, (B ... B ...)$_n$ and (C ... C ...)$_n$ molecules in the *a*-axis direction. The second amide group links chains together as (A ... C ... B ... A ...)$_n$. As such, all six amides are involved in regular, elegant amide···amide hydrogen bonds. The six amide ... amide interactions can be grouped into two categories with the shorter intrachain interactions as A ... A^{ii} = 2.924(4) Å, B ... B^{viii} = 2.973(4) Å, C ... C^{viii} = 2.865(4) Å (for the N···O distances) and are considerably shorter than the 3.078(4) Å, 3.289(4) Å and 3.029(5) Å for the interchain N···O distances of [C ... B ... A ... C^{ii}]$_n$. The pyridine-N atoms are at most involved in weaker C-H···N contacts (e.g., C35C-H35C···N32A^{ix}) augmenting the primary interactions. This is unusual, as *ortho*-N pyridine atoms usually form cyclic hydrogen-bonded rings, but this does not arise due to the plethora of amide···amide hydrogen bonds. Furthermore, there are two halogen···halogen contacts of note, namely Cl1B···Cl1C^{v} = 3.249(2) Å and Cl2B···Cl2C^{xv} = 3.308(2) Å (both of which are <3.50 Å, the van der Waals radii sum [15,28]) and a weak C25B-H25B···Cl1A^{xvi} hydrogen bonding contact (2.90 Å) as well as aromatic stacking. **Cl-DIP** demonstrates a snapshot of dynamic behaviour between three distinct conformations and with the ***syn*/*anti*** and ***anti*/*anti*** conformations isolated in the crystal structure. Of further note are the two Ru derivatives of **Cl-DIP** (with the N-H deprotonated and N atoms as donors) and one is a Ru^{II}(terpy)(**Cl-DIP**) structure [**CITDAL**] [23].

4.5. Br-DIP: A Wall of Bromine Atoms at the 2D Sheet Interfaces

Br-DIP is a twinned structure in space group *C*2/c and is isostructural with **F-DIP** (Figure 2), adopting the ***anti*/*anti*** conformation (Figure 4). **Br-DIP** molecules aggregate via reciprocal N1-H1···N32^{x} and C33-H33···N22^{x} interactions about inversion centres forming molecular pairs (with graph sets $R^2_2(7)$ and $R^2_2(20)$). This is similar to the pairs formed in **F-DIP**. In **Br-DIP**, hydrogen-bonded dimers are connected by N2-H2···O1^{xi} and C15-H15···O2^{xi} hydrogen bonds that cumulatively aggregate and form a sheet that is one molecule or ~20.4 Å wide (or 1/2 unit cell *a*-axis), and parallel with the *bc* plane (Figure 4).

Strong intermolecular interactions form within the sheet using both amides (N1-H1, N2-H2, O1, O2) and pyridines (N22, N32), together with additional C-H···O/N contacts. There are two sheets per unit cell intersecting at x = 0, 1/2 (midpoint at $x = \frac{1}{4}, \frac{3}{4}$). The sheet surface contains both terminal Br atoms (Br24, Br34) interspersed in a regular fashion as an array with the five shortest Br···Br distances in a range from 4.1 to 5.1 Å. Sheets are aligned so that Br···Br halogen bonding contacts arise with the shortest interfacial sheet distance being Br24···Br34^{xvii} = 3.6197(17) Å; 121.2(3)°, 155.7(3)° [N_c = 0.98] [14]. In addition, two Br34···Br34^{xviii,xix} distances are noted spanning the sheet interface and are 3.8534(14) Å and 3.8988(16) Å, respectively [14,15,28]. When the Hirshfeld surface is computed between two layers of molecules, the Br···Br contacts constitute 76% of the surface and Br···H$_C$ constitute 24%. One can speculate that sheets can glide over one another with relative ease. This may provide some rationale for the twinning in this crystal structure (additional diagrams of the **Br-DIP** sheets are provided; **ESI, Figures S5 and S6**). **F-DIP** differs from **Br-DIP** with unit cell wide sheets and **F-DIP** interfacial interactions comprising weak C-H···F contacts. The **Br-DIP** hydrogen bonding distances are mostly ca. 0.1 Å shorter than their **F-DIP** equivalents. However, the KPI packing index is 69.1 (**Br-DIP**) and 71.1 (**F-DIP**) as calculated using PLATON [28]. This small difference is accountable by small voids in proximity to the Br···Br interactions at the sheet interface in **Br-DIP** [14,27,28].

An overview of the **X-DIP** crystal structures suggests that **H-DIP** contains tight amide···pyridine and amide···amide interactions. The **F-DIP** and **Br-DIP** structures are essentially isostructural, but with key differences involving their F···H and Br···Br interactions at the 2D sheet interfaces, as shown for the wall of bromine atoms in Figure 4b. Of note is that **Cl-DIP** diverges in structure from the other three **X-DIPs** (H, F, Br) by having strong amide···amide hydrogen bonding interactions forming exclusively. The F, Cl and Br halogenated crystal structures all have walls of halogen···halogen interactions but the **Br-DIP** case is more pronounced, notably due to the larger size of the bromine atom.

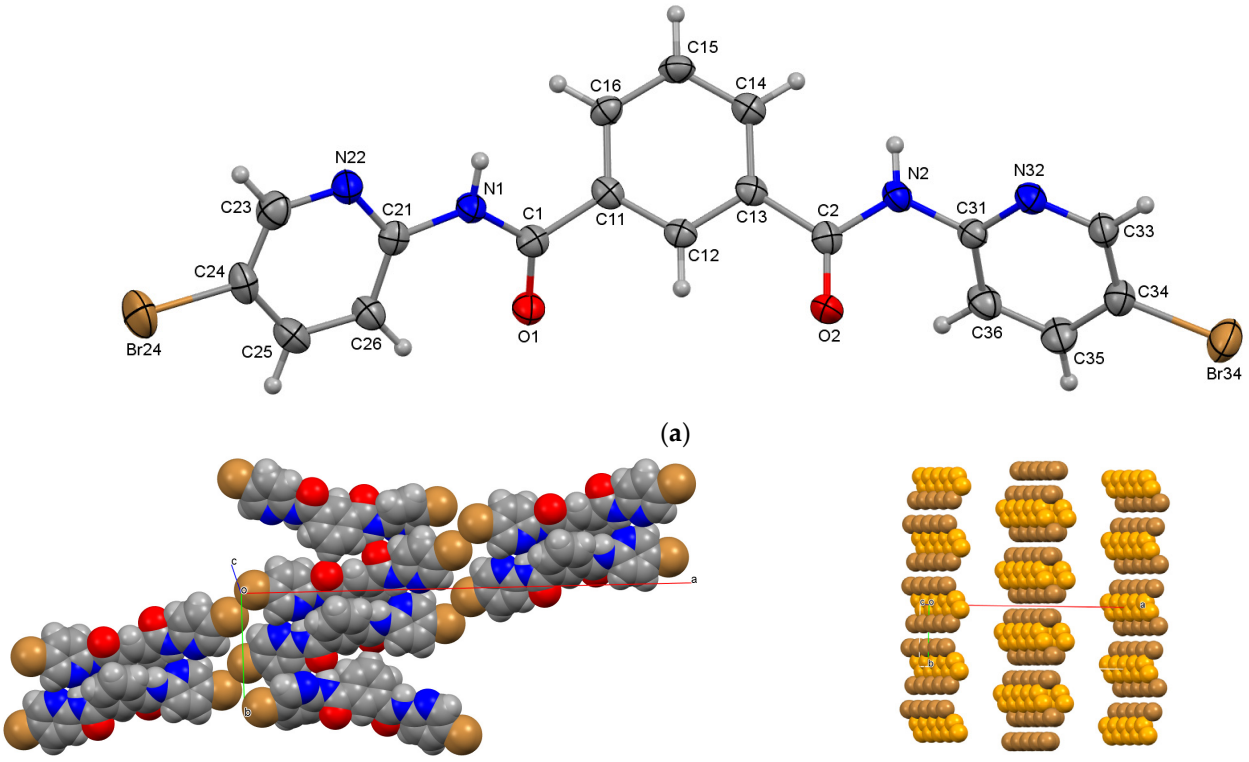

Figure 4. *Cont.*

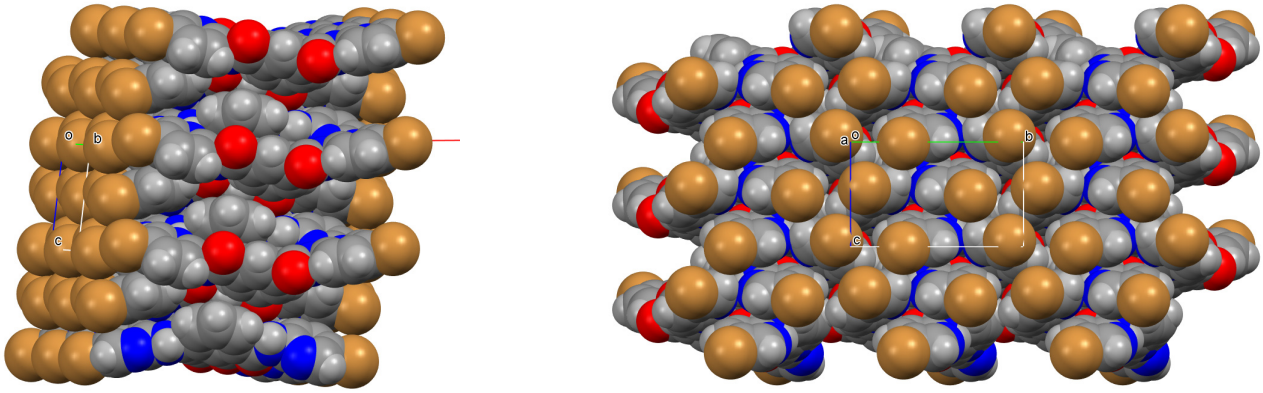

(**b**)

Figure 4. (**a**) An ORTEP view of **Br-DIP** with atoms depicted at 30% displacement ellipsoids. (**b**) CPK views of the (*i*) primary hydrogen and halogen bonding interactions, (*ii*) wall of bromines only with **Br24** (brown) and **Br34** (orange) and (*iii*, *iv*) two views of the wall of Br atoms on the bromine-rich sheet interface in the **Br-DIP** crystal structure (both Br as brown).

4.6. I-DIP•1/2 (H_2O): The N···I, I···I Halogen Bonding and Role of the Water Molecule

The **I-DIP** molecular structure adopts the ***syn*/*anti*** conformation and is comparable to **H-DIP** in molecular structure, although a hydrate is incorporated per **I-DIP** halogen-bonded dimer. The primary interactions driving the aggregation involve (*i*) amide···amide chain formation along the *b*-axis direction, (*ii*) a hydrogen-bonding synthon involving two aminopyridine groups and a water molecule that resides on twofold axes in a tightly bound arrangement, together with (*iii*) compact N22···I34 halogen bonding (N_c = 0.877) that drives **I-DIP** dimer formation [14] and further linked by the water, chain formation and aromatic stacking.

The primary hydrogen bonding in **I-DIP●**1/2(H_2O) is N1-H1···(O1=C1)^{vii} along the *b*-axis direction (with offset aromatic stacking forming a column). This is augmented by centrosymmetric N22···I34^{xiii} halogen bonding between pairs of chains to aggregate as a two-molecules (slipped) stack with a cyclical N22···I34^{xiii} assembly of $R^2_2(28)$ halogen-bonded rings. The iodinated compound is the only one among X-DIP to form N···X halogen bonds. The centrosymmetric C35-H35···O2=C2^{xiii} hydrogen bonds complement the N22···I34^{xiii} dimer formation [14]. Halogen bonding as I24···I34^{xx} = 3.8441(3) Å (N_c = 0.97) with C24-I24···I34^{xx} = 168.23(9)° and I24···I34^{xx}-C24^{xx} = 91.56(8)° is noted [14]. The O1W water molecule resides on a twofold axis and is tightly sandwiched between a pair of **I-DIP** molecules. It engages in hydrogen bonding to two amide N2-H2 donors and N32 pyridine acceptors (related by twofold symmetry: Figure 5a,b). There are also two weak C14-H14···O1W contacts per water molecule augmenting the stronger interactions. Centrosymmetric columns are linked by this hydrogen bonding involving (2 × N, N-H, C-H) and the O1W water molecule. Therefore, the O1W molecule interacts with two donors (as 2 × O1W-H1W) and as four acceptors (from 2 × N2-H2···O1W; 2 × C14-H14···O1W) and links the two-molecule columns into a sheet. The C14-H14···O1W is long but nonetheless a contributing hydrogen bonding contact (with normalised data for H14···O1W giving a H···O distance = 2.58 Å, C14-H14···O1W = 150°). The I24···I34^{xx}, C35-H35··· (O2=C2)^{xiii} and aromatic stacking interactions complete the 3D interactions (Figure 5c,d). The **I-DIP●**1/2(H_2O) packing does not display 2D layers of I···I interactions, but such interactions are only repeated along lines parallel to the *b* axis.

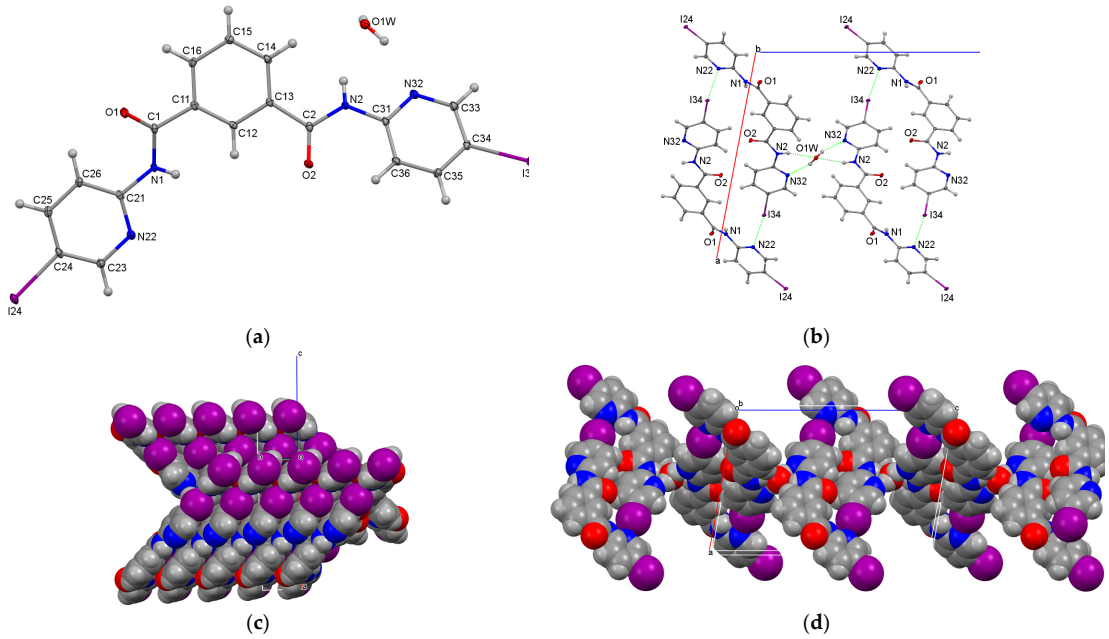

Figure 5. (**a**,**b**) An ORTEP plot of the **I-DIP**•1/2(H_2O) structure and a view of the hydrate in the assembly of the halogen-bonded dimers via an unusual synthon. (**c**,**d**) The stacking along the *b*-axis in the **I-DIP**•1/2(H_2O) structure and role of the water molecule linking two molecule stacks in the assembly process.

4.7. How Unusual Is the Water Environment in I-DIP•1/2(H$_2$O)?

The synthon involving the water molecule is uncommon although there are notable cases in the CSD [32]. For example, in **CIMTOI**, the ligand wraps around the H_2O molecule, resulting in two short O-H···N, two short N-H···O and two longer N-H···O hydrogen bonds [36]. In context, it is a relatively rare synthon to observe in *ortho*-amidopyridine (HN-C_5HN_4)-type structures as the tendency is for this group to form hydrogen-bonded dimers with graph set $R^2_2(8)$ as noted in an *ortho*-methyl-*N*-(2-pyridyl)benzamide (**Moo**) [17]. Insertion of a water molecule to disrupt this cyclic assembly is relatively rare [32]. In **UGARIE**, the water molecule is located such that it is involved in an excess of the usual [2D+2A] H_2O hydrogen bonding arrangement [37]. Another example (**MIJSII01**) highlights research on an unusual exotic state of a water molecule located in hydrophilic nanoconfined spaces [38].

4.8. CSD Analyses with the 2021.3.0 Version (January 2023)

A CSD search shows that there are 8446 *ortho*-aminopyridine (HNC_5N) fragments (hits) with 3D coordinates; 3509 with C-H. There are 3971 (47%) organic without a metal (4M) [32]. A total of 574 (7%) form hydrogen-bonded dimers (N . . . N within van der Waals limits). There are several notable examples of the (N, $NH)_2$•OH_2-type synthon present in the **CIMTOI**, **ESALES**, **MONGON**, **SEMGEY** and **WAMSOT** structures [32]. It can be shown that this represents only <1% of these general-type structures. Incorporation of a water molecule to disrupt 'aminopyridine dimer' formation is therefore unusual. Statistics do not vary much from analyses using datasets from the earlier versions of the CSD. An analogous study of carboxylic acid structures as C-CO_2H with 3D coordinates shows similar statistics when compared with organic carboxylic acids without 4M dimer formation and also checking for H_2O insertion between the carboxylic acids (as for pyridine above).

5. Comparisons with Related Structures

The isostructural *N*,*N*′-bis(4-halophenyl)pyridine-2,6-dicarboxamides **TOYQIJ** (**F-pyr**) [35] and **MEWNEJ** (**Br-pyr**) [39] in space groups $P2_1/c$ and $C2/c$, respectively, differ

from **F-DIP** and **Br-DIP** by replacing the central aromatic $_{ipso}$C-H with N. This difference enforces ***syn*/*syn*** conformations on **TOYQIJ** and **MEWNEJ** via a relay of intramolecular N-H···N···H-N interactions and contrasting with the ***anti*/*anti*** conformations in **F-DIP** and **Br-DIP**. As noted from our **X-DIP** structures, the $_{ipso}$C-H exerts both steric and electronic effects on the neighboring amido N-Hs and does not promote intramolecular hydrogen bonding apart from weak C-H···O=C hydrogen bonds. Therefore, the $_{ipso}$C-H moiety does not form strong intramolecular hydrogen bonding, and this facilitates the relatively free rotation about the C_6-amide bond from the ***syn*/*syn*** to ***anti*/*anti*** conformation via ***syn*/*anti***.

6. Crystallographic Structural Summary

Although the ***syn*-*syn*** conformation is the most stable conformation, the **H-DIP**, **I-DIP** and **Cl-DIP** (molecules B, C) have the ***syn*-*anti*** conformation, whereas the **F-DIP**, **Cl-DIP** (molecule A) and **Br-DIP** adopt ***anti*-*anti*** conformations. The five crystal structures aggregate by similar intermolecular interactions due to their overall molecular similarities (varying only by the terminal aromatic *para*-H to *para*-I relative to the amide group). Amide···amide hydrogen bonding dominates as the main hydrogen bonding interaction responsible for aggregation with an N_c value $\approx$ 0.81 for the **Cl-DIP**, **Br-DIP** and **I-DIP●**$^1/_2$(H_2O) structures, while in **H-DIP** and **F-DIP**, the amide ... amide interaction is less notable (N_c values $\geq$ 0.90). In tandem, the $R^1_2(7)$ bifurcated interaction from the C=O···H–N interaction and central C_6 ring C–H (as C=O···H–C) is present in all crystal structures, except for **I-DIP●**$^1/_2$(H_2O). Moreover, the N–H···$N_{pyridine}$ hydrogen bonding dominates in **F-DIP** as the N-H···O interaction is weaker with a relatively long H···O distance of 2.488 Å. Despite their structural similarities, each compound exhibits its own unique intermolecular interactions. For **H-DIP**, ring···ring interactions play a crucial role in aggregation by both phenyl···pyridine stacking and pyridine···pyridine ring stacking. Additionally, the **F-DIP** and **Br-DIP** compounds exhibit a larger amount of C–H···F interactions and Br···Br contacts, respectively. In **I-DIP●**$^1/_2$(H_2O), the I···$N_{pyridine}$ halogen bonding interaction is present, in addition to weaker I···I contacts with C34-I34···I24 = 91.56(8)°. The water solvate also plays a crucial role in aggregation.

In previous studies of 3 × 3 isomer grids, we reported detailed analyses of their melting points and examined the influence of the substituent position and molecular symmetry [17–19,40]. The **X-DIP** series with six compounds shows a melting point trend increasing along the series from H→F→Cl→Br→I→NO_2, noting Z' = 3 for **Cl-DIP** and hemihydrate in **I-DIP●**$^1/_2$(H_2O). The average melting point changes from 184 °C (**H-DIP**), 224 °C (**F-DIP**), 236 °C (**Cl-DIP**), 246 °C (**Br-DIP**), 265 °C$_{decomp}$ (**I-DIP●**$^1/_2$(H_2O) to 300 °C$_{decomp}$ (**NO_2-DIP**). This is expected on increasing molecular weights in the **X-DIP** series. Of note is the recent study examining the lowering of melting points in deformed plastic crystals [41] and would be of interest if extended to crystals with Z' > 1 and isomorphous structures [20,32].

7. Fingerprint and Contact Analysis

All five crystal structures were analyzed using fingerprint analysis (**ESI**). It has to be noted that for the **Cl-DIP** (Z' = 3) structure, a set of separated molecules was analyzed globally (Hirshfeld surfaces around three molecules not in contact in order to have an integral surface around each molecule). For **I-DIP●**$^1/_2$(H_2O), the hemihydrate molecule is not included in the crystal packing.

8. Contacts Statistics on the Hirshfeld Surface

The Hirshfeld surface represents the region where molecules come into contact. The contact surface is attributed to pairs of chemical species X and Y in mutual contact. The contacts' enrichment and derived ratios are in the **ESI part II**, as computed with MoProViewer [34].

The strong hydrogen bonds O···H_P and N···H_P involving the H-N (and water H-O in the **I-DIP**•1/2(H_2O) structure) polar hydrogen atoms are nearly always significantly over-represented at enrichments $E > 3$ (Figure 6b). The only exception occurs for the chlorinated **Cl-DIP** structure, where, despite the presence of three independent molecules, all the strong H bonding occurs only in N-H···O interactions ($E = 9.9$). The weaker hydrogen bonds H_C···O and H_C···N do also occur; they are generally also over-represented but with E values closer to unity (extreme values are 0.55 and 2.43 for **I-DIP**•1/2(H_2O).

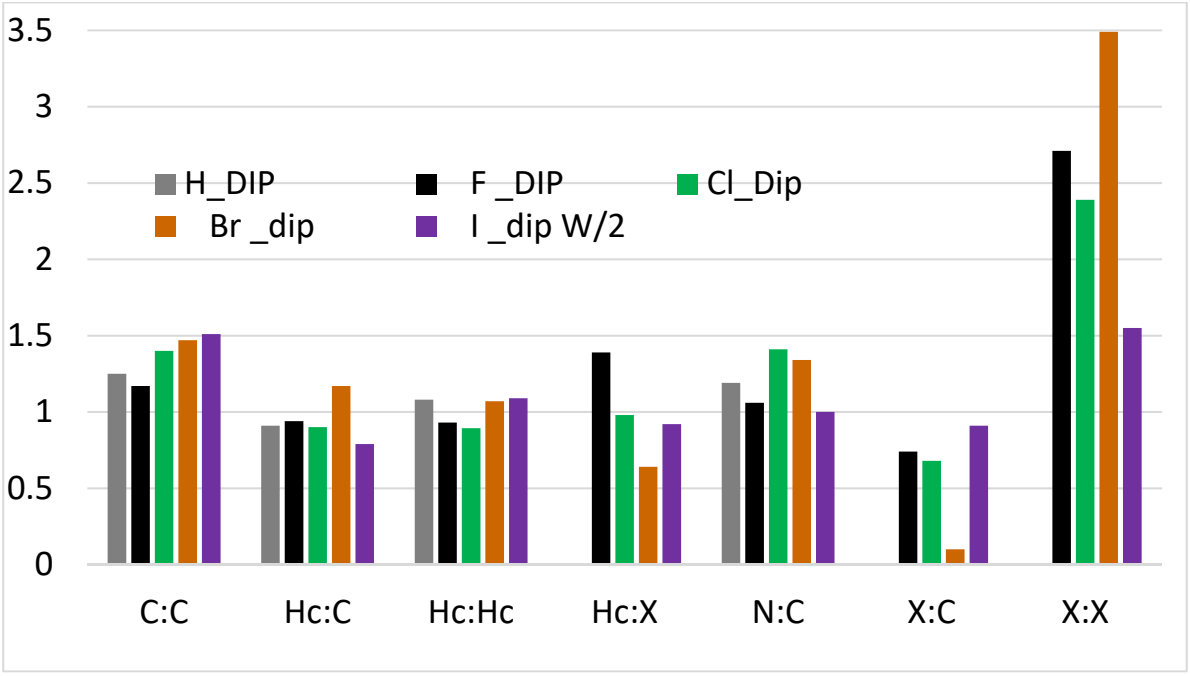

(**a**)

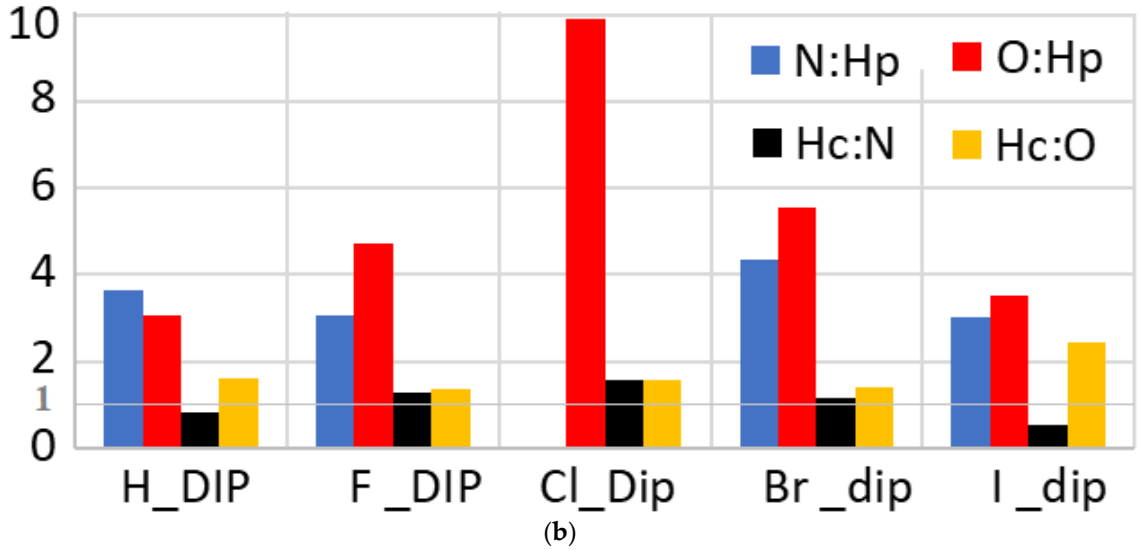

(**b**)

Figure 6. (**a**) Enrichment of the hydrophobic contacts and (**b**) enrichment of hydrogen bonds. H_C and H_P refer to the hydrophobic H-C and the polar hydrogen (H-N and H-O) atoms, respectively.

The enrichment of hydrophobic contacts between C, H_C and halogen X atoms are shown in Figure 6a. The X···X contacts appear to be the most favoured hydrophobic interaction in the four halogenated compounds and the highest enrichment ratio reaches 3.5 for the **Br-DIP** crystal (Table S4). The halogen···halogen contacts in relation to the molec-

ular geometry are discussed in more detail in the enriched halogen···halogen contacts section below.

The C···C and N···C contacts are always slightly enriched (E between 1.0 and 1.5) which denotes the occurrence of aromatic stacking in the five **DIP** structures. Aromatic stacking is generally favoured in aromatic heterocycles as the presence of electropositive and electronegative atoms on the aromatic rings allows attractive electrostatic interactions between adjacent cycles [42,43]. H_C···H_C contacts have limited enrichments which remain close to unity as competition arises with X···H_C, N···H_C and O···H_C weak H bonds. The C···H_C contacts also exhibit limited E values close to one, as all compounds show significant aromatic stacking. They are essentially van der Waals contacts (between aromatic rings that are not far from being parallel) rather than C-H···π weak hydrogen bonds.

In statistical studies of the interaction propensities in crystal structures of halogenated compounds [44,45], it was observed that H_C atoms are generally the favoured interaction partners for organic halogen atoms, which are hydrophobic in nature. The X···H-C weak hydrogen bonds do occur in all four halogenated crystal structures but are over-represented only in the **F-DIP** case. The Br···H_C contacts are particularly disfavoured (E_{BrHc} = 0.64) in the **Br-DIP** crystal structure which instead displays high Br···Br contact enrichment (Table S4). It can be seen in Figures S5 and S6a–e (**ESI**), that the bromine atoms interact almost only with Br atoms and to a small extent with the H_C hydrogen atoms.

9. Enriched Halogen···Halogen Contacts

The Br, F and **Cl-DIP** compounds display all layers in the crystal packing formed by halogen atoms forming many frontal and lateral contacts. These halogen layers may be related to the *para*- position of the halogen atoms, at the extremities of the molecules which are nearly linear for the Br, F and Cl crystal structures (Figures 2–4). The **Br-DIP** crystal has, for instance, all molecules oriented along the *a*-axis direction, which is the longest unit cell axis (40.80 Å). There are layers of Br atoms in the planes $x = n$ and $x = n + 1/2$. The situation is the same in **Cl-DIP** crystal where c is the longest unit cell axis (33.83 Å) and the Cl layers are located at $z = n$ and $z = n + 1/2$. In the case of **F-DIP**, molecules are oriented along a, the long unit cell axis, but there are layers of F atoms only in the planes $x = n$ as the a-axis is not so long (17.94 Å). The halogen···halogen interactions in these layers are all of type II (C1-X1···X2 ≈ C2-X2···X1) where the two halogen atoms minimize repulsion by interfacing the neutral regions of their electrostatic potential surfaces [46].

On the contrary, the **I-DIP**•$1/2(H_2O)$ and **H-DIP** compounds (Figures 1 and 5a–d) do not have a global linear shape but are bent (***syn-*/*anti-*** conformations). In **I-DIP**•$1/2(H_2O)$, the iodine atoms are not located in crystalline layers, but are located along rows parallel to the short unit cell axis b. The shortest I···I contact has type II geometry [47] with ∠C34-I34···I24 = 91.56(8)° ≈ 90° and C24-I24···I34^{xx} = 168.23(9)° near linearity (180°) and is an electrophilic (σ-hole)···nucleophilic interaction. In addition, longer I···I-type contacts are present.

By analogy, there are several other crystal structures of elongated molecules with aryl groups halogenated in the *para* position as detailed in the CSD [32]. Among the four *para*-dihalo-benzene crystals, the $C_6H_4F_2$ [48] and $C_6H_4Cl_2$ (**ZZZPRO05**; [32]) compounds also show plane layers of halogen atoms.

Among the four 4,4′-di-halo-biphenyl compounds, which are elongated molecules with halogen atom in *para* positions, the iodinated [49] and fluorinated [50] compounds show plane layers constituted by the halogen atoms. The molecules in the crystal display two orientations but the line between the two halogen atoms is always oriented in the same direction. The chlorinated and brominated compounds show head-to-tail X···X contacts, but the halogen atoms are distributed in unidimensional rows. Para-difluoro benzamide is also a typical example of such packing [51]. The 4-fluoro-*N*-(4-fluorophenyl)benzamide molecules are all aligned in space group *P*-1 (No. 2) along the *c*-axis corresponding to the longest unit cell axis and the crystal has layers of fluorine atoms around planes $z = n + 1/2$.

In the study of contact propensities in the crystal structures of halogenated organic molecules [44], the packing of the $C_{22}H_{12}Br_2$ molecule (**OKANOE** [32,52]) was identified as having a particularly high Br···Br contact enrichment. The molecule 2,3-dibromopentacene is a very long rigid elongated molecule bearing two Br atoms on its extremities where the shape of the molecule plays an essential role in the crystal packing formation. The packing shows the typical elongated unit cell with layers of bromine atoms (together here with H_C atoms) around planes $z = n$ and $z = n + 1/2$.

In related halogen bonding research, the effect of temperature on isostructural triethyl-tris(4-halophenoxy)-methylbenzenes shows that the increase in interhalogen distance on increasing temperatures is the reverse order of the strength of the interhalogen interaction [53]. Recently, in an elegant study, the differences in thermal expansion and motion ability were reported for a series of (di)imines, (di)olefins and di(azo) derivatives. Herringbone packing and face-to-face π stacking were studied and key differences in expansion and motion were analysed [54]. In comprehensive melting point analyses, we have shown that the substituent position is more important than the nature of the substituent in a series of 3 × 3 benzamide isomer grids [17–19]. Together, these and other studies highlight the complex considerations needed in the design and structures of new materials, especially those containing halogen atoms [14,32].

10. Structure Optimization—Ab Initio Calculations

The **X-DIP** molecules were modelled in *gas phase* using DFT (B3LYP/6-311++G**) methods [30,31] and only the **I-DIP** molecule was optimised by several semi-empirical methods (AM1, PM3, MNDO), then optimised by the (B3LYP/3-21G) method due to the difficulty in using (B3LYP/6-311++G**) for iodo-containing molecules [30,31,55,56]. The main geometric parameters are the (*i*) *α*-dihedral C12–C11–C1=O1 angle, (*ii*) *β*-dihedral C1–N1–C21–C26 and (*iii*) *γ* or amide dihedral angle H1–N1–C1=O1. On the opposite side of the **DIP** structures are the (*iv*) *α*-dihedral C12–C13–C2=O2 angle, (*v*) *β*-dihedral C2–N2–C31–C36 and (*vi*) *γ* or amide dihedral angle H2–N2–C2=O2, with all six angles tabulated in Tables 3 and 4.

Table 3. Torsion angles (°) of the optimized **X-DIP**s by DFT (B3LYP/6-311++G**) method.

Dihedral Angle	O1–C1–C11–C12 (α1)	C1–N1–C21–C26 (β1)	O1–C1–N1–H1 (γ1)	O2–C2–C13–C12 (α2)	C2–N2–C31–C36 (β2)	O2–C2–N2–H2 (γ2)	Molecular Energy (10^3 kJ mol^{-1})
H-DIP	152.38	−4.12	171.73	152.38	−4.12	171.73	−2793.9
F-DIP	152.31	−4.04	171.68	152.31	−4.04	171.67	−3315.1
Cl-DIP	152.53	−3.98	171.68	152.53	−3.98	171.69	−5207.4
Br-DIP	152.43	−3.98	171.63	152.43	−3.97	171.63	−16,307.6
NO_2-DIP	152.48	−4.00	171.18	152.48	−3.98	171.20	−3868.04

Table 4. Torsion angles (°) of the optimized **I-DIP** conformations by DFT (B3LYP/3-21G) method.

I-DIP	O1–C1–C11–C12 (α1)	C1–N1–C21–C26 (β1)	O1–C1–N1–H1 (γ1)	O2–C2–C13–C12 (α2)	C2–N2–C31–C36 (β2)	O2–C2–N2–H2 (γ2)	Molecular Energy (10^3 kJ mol^{-1})
syn-syn	170.73	−0.41	175.15	170.72	−0.40	175.51	−38,982.94
syn-anti	−13.20	164.03	163.25	−178.75	0.04	−179.41	−38,982.73
anti-anti	−17.65	161.91	161.16	−17.65	161.91	161.16	−38,982.84

The six **DIP** compounds were optimized to the lowest energy structure having the ***syn-syn*** conformation (Figure 7). This is shown in Figure 8 (as the Potential Energy Scans or PES diagram) and only the **I-DIP** structure was optimized as the ***syn-syn***, ***syn-anti*** and ***anti-anti*** conformations. In the ***syn-syn*** conformation, the outer pyridine rings are not co-planar with the central aromatic ring and rotated by ~28°, while they are almost co-planar with the amide linkages (~4° deviation). Additionally, the amide linkages are planar as expected (Table 3) with γ1 and γ2 values of ~171°. The different substituents do not affect

the molecular geometries, which is expected, since the substituents are *para*-related relative to the amide linkage. However, the crystal structures showed the effect of these substituents on intermolecular interactions. The molecular energies decrease in the expected order since the negative interaction energy increases with the enhancement of halogen bonding, which has the lowest value in the presence of iodine. This explains the small differences in energy between **F-DIP**, **NO_2-DIP** and **H-DIP** compared with the other halogens [57–59]. Moreover, the crystal structures reveal the increase in halogen···halogen intermolecular interactions as noted by the Cl···Cl contacts in the **Cl-DIP** structure and Br···Br contacts in **Br-DIP** and ultimately both N···I halogen bonding and I···I contacts in the **I-DIP** structure. For **I-DIP**, optimization of the three different conformations reveals the ***syn-syn*** conformation to have the lowest molecular energy and ***syn-anti*** to have the highest.

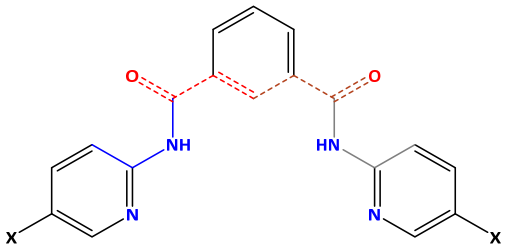

Figure 7. The **X-DIP** structure showing the torsion angles as analyzed.

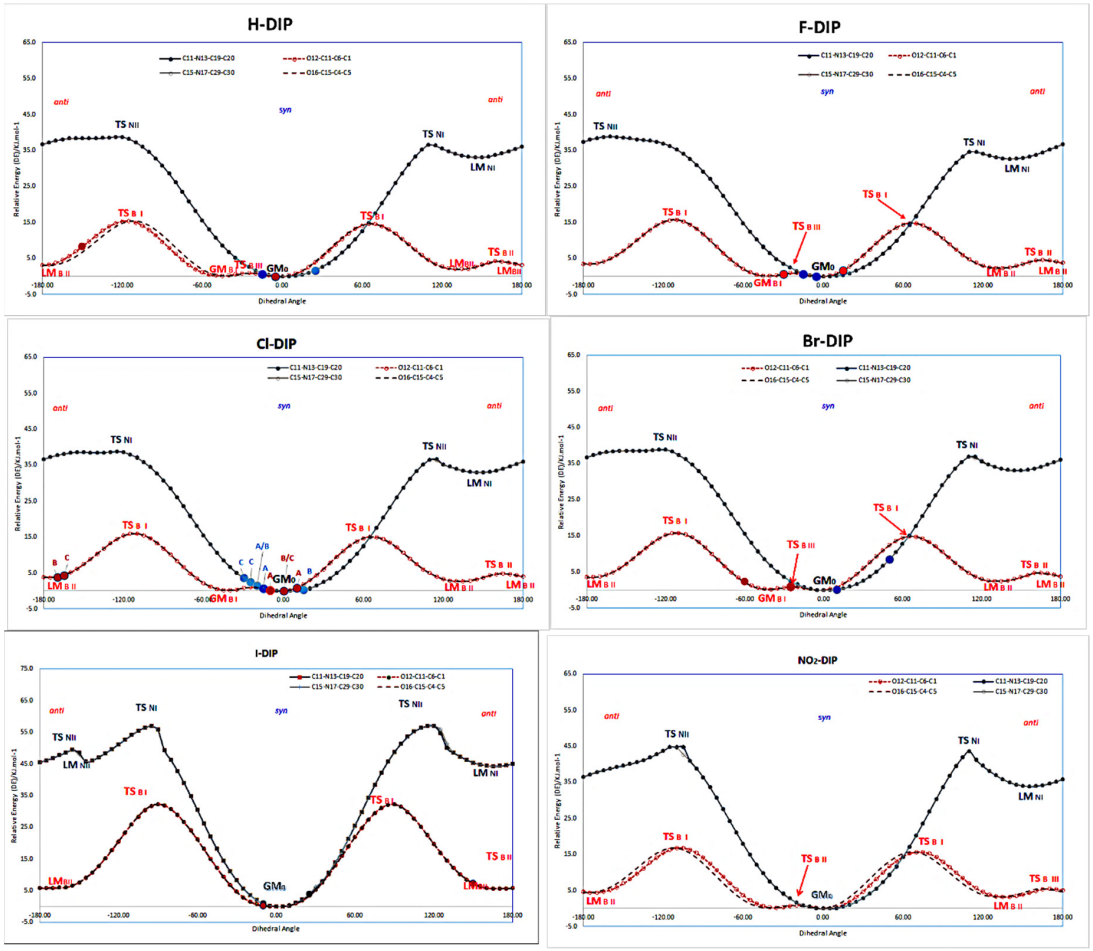

Figure 8. Conformational analyses of the **X-DIP** molecules: the equivalent solid-state angle is shown with an identification letter and/or occupancy (%) if required. **I-DIP** is represented without the hemihydrate and data are not available for **NO_2-DIP**.

The ***anti-anti*** conformation in **I-DIP** shows the pyridine rings to be almost perpendicular to the phenyl ring while the carbonyl groups are not co-planar. The amide bridges retain planarity (as expected) and with the ***syn-syn*** conformation resulting in a highly planar structure. The ***syn-anti*** conformation, though, shows a slight deviation from planarity in the ***anti*** component and complete planarity for the ***syn*** side. Despite the different geometries between the ***syn-syn*** and the ***anti-anti*** conformation, their energies vary within a few kJ and are to be discussed in the conformational analysis section.

11. Conformational Analysis

Conformational analysis is a useful approach to understand the relationships between energy and geometry [17–20]. The possibility of attaining different conformational preferences as influenced by steric and electronic factors may be realised by varying the position of carbonyl groups relative to the aromatic rings and to the position of the N atom in the pyridine rings (Figure 7). Because the substituents atoms are located *para*, the effect of pyridine ring rotation is not influenced by the *para*-substituent nature. Only the position of the pyridine ring with respect to the amide linkage is responsible for the change in the energy as shown in PES diagrams (Figure 8) as represented by a **blue curve**. The lowest energy is obtained by having the $N_{pyridine}$ in the opposite direction to the carbonyl group and planar with the amide linkage. The rotation of the pyridine ring in the ***syn-syn*** conformation to the perpendicular position increases the molecular energy (TS_{NI}) by 36.5 ± 0.5 kJ mol^{-1} (as for **F-DIP** increasing to 34 kJ mol^{-1} and for **NO_2-DIP** to 44 kJ mol^{-1}). If the rotation occurs with the $N_{pyridine}$ in the same direction of the carbonyl group, it increases the energy of molecule (TS_{NII}) by 38.1 ± 0.5 kJ mol^{-1} (only **NO_2-DIP** increases to 44 kJ mol^{-1}). In **I-DIP,** the energy increase reaches 56.8 kJ mol^{-1}and 57 kJ mol^{-1}, respectively. This highlights and ties in with the analysis of the **X-DIP** crystal structures that their torsion angles are always close to the global minimum point (Figure 8).

The rotation of the carbonyl group around the phenyl ring as represented by the **red curve** in the PES (Figure 8) is found to be more flexible since the maximum transition point is 15.8 ± 1 kJ mol^{-1} in all ***syn-syn*** conformations and can be observed in the crystal structure torsion angles of **H-DIP** and **Cl-DIP**. The corresponding transition energy doubles in **I-DIP**. The PES for the **X-DIP** compounds shows the lowest energy molecule to adopt the ***syn-syn*** conformation, then the ***anti-anti*** conformation, as noted in the **F-DIP** and **Cl-DIP** (molecule A) structures. Although the ***syn-anti*** conformation is found to have a relatively high energy compared with the other two conformations, it is seen in the **H-DIP**, **Cl-DIP** (molecules B, C) and **I-DIP** crystal structures. Differences between the ***syn-syn*** and ***syn-anti*** conformations do not exceed 5.0 kJ mol^{-1}; however, the difference between the ***anti-anti*** and ***syn-anti*** conformation varies by up to 10 kJ mol^{-1}.

12. Conclusions, Insights and Future Work

Isophthalamides are an interesting group of molecules that provide a diverse range of structural types as noted in their crystal structures. The development of molecules with functional groups and directing components to facilitate subtle structural changes is of interest. The crystal and model structures of the N^1,N^3-di(pyridin-2-yl)isophthalamide **H-DIP** and four N^1,N^3-bis(5-**X**-pyridin-2-yl)isophthalamides (**X** = F, Br, Cl, I) as **X-DIP** are reported, with an assessment of the roles which their molecular conformations and interactions play in solid-state aggregation. Peculiarly, **Cl-DIP** (Z' = 3) exhibits two different ***syn*/*anti*** and ***anti*/*anti*** molecular conformations. The hydrogen bonding hierarchy and sheet formation in **Br-DIP** creates a bromine-rich environment that manifest as a 'wall of bromine atoms' at the 2D sheet interfaces (**ESI**: Figures S5 and S6a,b). This leads to the possibility for use as potential model structures for bromine-rich surface environments and interfaces in materials science structures. The **Br-DIP** crystal structure is reminiscent of the lead(II) bromide and copper(II) bromide structures as presented for $PbBr_2$ in Figure S6d [60,61]. For **I-DIP**•$^1/_2$(H_2O), the hemihydrate forms a rare synthon involving a water molecule sandwiched between two **I-DIP** molecules. The **X-DIP** compounds are being

further modified with the development of new mixed amide-imide and di-imide systems of interest in several research areas [62].

Much research has gone into understanding intermolecular interactions such as halogen bonding in order to facilitate the construction of new materials [14,32,63]. When presented with a rare type of structural feature, it can promote a new direction in a research program. The changing of H by F is feasible and in many X-ray crystal structures does not yield a different structural type e.g., in fluorobenzamides [18]. A small and subtle shift of changing the *meta*-H to a *meta*-F atom in the bromopyridine ring in **Br-DIP** may be able to facilitate the wall of bromines being augmented by F atoms in the indentations, thereby further enhancing of the halogen-rich interface [14,63]. Model compounds such as this can be useful in designing new materials, or at least be used to study interesting, halogenated surfaces.

Contact enrichment analysis on the Hirshfeld surface pinpoints that the F, Br, **Cl-DIP** compounds have very over-represented halogen . . . halogen interactions [14,46]. In the crystal packing of the **F-DIP**, **Cl-DIP** and **Br-DIP** compounds, the molecules have an elongated skeleton and form layers of halogen atoms in planes perpendicular to the long unit cell axis. This kind of behaviour is often observed in elongated molecules which are halogenated at their extremities and may prove useful in the future design of new layered materials with specific functionalities.

Supplementary Materials: The following supporting information can be downloaded at https://www.mdpi.com/article/10.3390/sym15030738/s1. Crystallographic data for the five **X-DIP** crystal structures are deposited with the Cambridge Crystallographic Data Centre, CCDC numbers 2171172 to 2171177. The **Cl-DIP** structural data have been collected using both Cu (2171174) and Mo (2171175) radiation. CIF data may be accessed from the CCDC. Data are available as CIF files from the corresponding author in DCU—J.F.G. ESI_Part-1_Synthesis. Enlarged Figure 8 and Optimized structures. ESI_Part-2_Structures. Table S1 (Crystal Structure Experimental details). Table S2 (Selected hydrogen-bond parameters). Table S3 (The X-DIP melting point ranges); CSD studies and parameters. Figures S1–S7: (for the H-DIP, F-DIP, Cl-DIP, Br-DIP and I-DIP·0.5(H2O) structures. Figure S8: Contact types on the Hirshfeld surfaces of Cl-DIP. Table S4: Hirshfeld Surface content SX, actual contacts CXY and enrichment ratios EXY. Figure S9: Views of the five X-DIP crystals as mounted prior to data collection. ESI_Part-3_Fingerprint plots. Finger plots for the X-DIPS.

Author Contributions: I.A.O.: synthesis, methodology, molecular modelling, software, analysis; V.M.: data collection, structure solution, refinement, crystal structure analysis; V.M. and J.F.G.: design, crystal structure analysis, data curation, writing and editing; C.J.: contacts analysis, Hirshfeld analysis, writing and editing. All authors have read and agreed to the published version of the manuscript.

Funding: This research received no external funding.

Data Availability Statement: Additional data pertaining to this publication are available in the ESI.

Acknowledgments: Acknowledgments J.F.G. and I.A.O. thank Dublin City University for research chemical funding. We hereby thank Pavle Mocilac (Department of Nuclear Science & Technology, Lanzhou University, Gansu, China) and Niall Hehir (APC Ltd.) for discussions on supramolecular chemistry and ligand/macrocyclic syntheses over several years of postgraduate research.

Conflicts of Interest: The authors declare that they have no known competing financial interests or personal relationships that could have appeared to influence the research work as reported in this scientific paper.

References

1. Constable, E.; Parkin, G.; Que, L. (Eds.) *Comprehensive Coordination Chemistry III*, 3rd ed.; Elsevier: Amsterdam, The Netherlands, 2021; ISBN 9780081026885.
2. Stradiotto, M.; Lundgren, R.J. *Ligand Design in Metal Chemistry*; J. Wiley & Sons Ltd.: Hoboken, NJ, USA, 2016. [CrossRef]
3. Storr, T. (Ed.) *Ligand Design in Medicinal Inorganic Chemistry*; J. Wiley & Sons Ltd.: Hoboken, NJ, USA, 2014. [CrossRef]
4. Silverman, R.B.; Holladay, M.W. *The Organic Chemistry of Drug Design and Drug Action*, 3rd ed.; Academic Press: Cambridge, MA, USA, 2014. [CrossRef]

5. Malone, J.F.; Murray, C.M.; Dolan, G.M.; Docherty, R.; Lavery, A.J. Intermolecular Interactions in the Crystal Chemistry of *N,N′*-Diphenylisophthalamide, Pyridine-2,6-dicarboxylic Acid Bisphenylamide, and Related Compounds. *Chem. Mater.* **1997**, *9*, 2983–2989. [CrossRef]
6. Gondi, S.R.; Son, D.R. Synthesis of *N,N′-bis*(2-Thiazolinyl)-, *N,N′-bis*(2-Thiazolyl)-, and *N,N′-bis*(2-Pyrimidinyl)-Benzene Dicarboxamides. *Synth. Commun.* **2004**, *34*, 3061–3072. [CrossRef]
7. Odago, M.O.; Hoffman, A.E.; Carpenter, R.L.; Chi Tak Tse, D.; Sun, S.S.; Lees, A.J. Thioamide, urea and thiourea bridged rhenium(I) complexes as luminescent anion receptors. *Inorg. Chim. Acta* **2011**, *374*, 558–565. [CrossRef]
8. Zhang, D.W.; Zhao, X.; Hu, J.L.; Li, Z.T. Aromatic Amide Foldamers: Structures, Properties, and Functions. *Chem. Rev.* **2012**, *112*, 5271–5316. [CrossRef]
9. Yashima, E.; Ousaka, N.; Taura, D.; Shimomura, K.; Ikai, T.; Maeda, K. Supramolecular Helical Systems: Helical Assemblies of Small Molecules, Foldamers, and Polymers with Chiral Amplification and Their Functions. *Chem. Rev.* **2016**, *116*, 13752–13990. [CrossRef]
10. Ferrand, Y.; Huc, I. Designing Helical Molecular Capsules Based on Folded Aromatic Amide Oligomers. *Acc. Chem. Res.* **2018**, *51*, 970–977. [CrossRef]
11. Desiraju, G.R.; Steiner, T. *The Weak Hydrogen Bond in Structural Chemistry and Biology*; Oxford University Press: Oxford, UK, 2001.
12. Martinez, C.R.; Iverson, B.L. Rethinking the term "pi-stacking". *Chem. Sci.* **2012**, *3*, 2191–2201. [CrossRef]
13. Alvarez, S. A cartography of the van der Waals territories. *Dalton Trans.* **2013**, *42*, 8617–8636. [CrossRef] [PubMed]
14. Desiraju, G.R.; Ho, P.S.; Kloo, L.; Legon, A.C.; Marquardt, R.; Metrangolo, P.; Politzer, P.; Resnati, G.; Rissanen, K. Definition of the halogen bond (IUPAC Recommendations 2013). *Pure Appl. Chem.* **2013**, *85*, 1711–1713. [CrossRef]
15. Politzer, P.; Murray, J.S. The use and misuse of van der Waals radii. *Struct. Chem.* **2021**, *32*, 623–629. [CrossRef]
16. McMahon, J.; Gallagher, J.F.; Anderson, F.P.; Lough, A.J. A structural systematic study of four isomers of difluoro-*N*-(3-pyridyl)benzamide. *Acta Crystallogr.* **2009**, *C65*, 345–351. [CrossRef] [PubMed]
17. Mocilac, P.; Tallon, M.; Lough, A.J.; Gallagher, J.F. Synthesis, structural and conformational analysis of a 3 × 3 isomer grid based on nine methyl-*N*-(pyridyl)benzamides. *CrystEngComm* **2010**, *12*, 3080–3090. [CrossRef]
18. Mocilac, P.; Donnelly, K.; Gallagher, J.F. Structural systematics and conformational analyses of a 3 × 3 isomer grid of fluoro-N-(pyridyl)benzamides: Physicochemical correlations, polymorphism and isomorphous relationships. *Acta Crystallogr.* **2012**, *B68*, 189–203. [CrossRef] [PubMed]
19. Gallagher, J.F.; Farrell, M.; Hehir, N.; Mocilac, P.; Aubert, E.; Espinosa, E.; Guillot, B.; Jelsch, C. At the Interface of Isomorphous Behavior in a 3 × 3 Isomer Grid of Monochlorobenzamides: Analyses of the Interaction Landscapes via Contact Enrichment Studies. *Cryst. Growth Des.* **2019**, *19*, 6141–6158. [CrossRef]
20. Mocilac, P.; Gallagher, J.F. Monohalogenated carbamates where hydrogen bonding rules without halogen bonding: Is there a link between poor carbamate crystal growth and $Z' > 1$? *CrystEngComm* **2019**, *21*, 4048–4062. [CrossRef]
21. Khavasi, H.R.; Tehrani, A.A. Effect of halogen bonding interaction on supramolecular assembly of halogen-substituted phenylpyrazinamides. *CrystEngComm* **2013**, *15*, 3222–3235. [CrossRef]
22. Abeysekera, A.M.; Day, V.W.; Sinha, A.S.; Aakeröy, C.B. Mapping out the Relative Influence of Hydrogen and Halogen Bonds in Crystal Structures of a Family of Amide-Substituted Pyridines. *Cryst. Growth Des.* **2020**, *20*, 7399–7410. [CrossRef]
23. Dasgupta, M.; Nag, S.; Das, G.; Nethaji, M.; Bhattacharya, S. *N,N′*-Bis(aryl)pyridine-2,6-dicarboxamide complexes of ruthenium: Synthesis, structure and redox properties. *Polyhedron* **2008**, *27*, 139–150. [CrossRef]
24. Møller, M.S.; Liljedahl, M.C.; McKee, V.; McKenzie, C.J. Solid phase nitrosylation of enantiomeric cobalt(II) complexes. *Chemistry* **2021**, *3*, 585–597. [CrossRef]
25. Osman, I.A. Chapter 3. Ph.D. Thesis, Dublin City University, Dublin, Ireland, 2021.
26. Sheldrick, G.M. A short history of SHELX. *Acta Crystallogr.* **2008**, *A64*, 112–122. [CrossRef]
27. Macrae, C.F.; Sovago, I.; Cottrell, S.J.; Galek, P.T.A.; McCabe, P.; Pidcock, E.; Platings, M.; Shields, G.P.; Stevens, J.S.; Towler, M.; et al. *Mercury 4.0*: From visualization to analysis, design and prediction. *J. Appl. Crystallogr.* **2020**, *53*, 226–235. [CrossRef] [PubMed]
28. Spek, A.L. Single-crystal structure validation with the program PLATON. *J. Appl. Crystallogr.* **2003**, *36*, 7–13. [CrossRef]
29. Frisch, M.J.; Trucks, G.W.; Schlegel, H.B.; Scuseria, G.E.; Robb, M.A.; Cheeseman, J.R.; Scalmani, G.; Barone, V.; Mennucci, B.; Petersson, G.A.; et al. *Gaussian 09 Revision B.01*; Gaussian Inc.: Wallingford, CT, USA, 2010.
30. Becke, A.D. Density-Functional Thermochemistry. 3. The Role of Exact Exchange. *J. Chem. Phys.* **1993**, *98*, 5648–5652.
31. Krishnan, R.; Binkley, J.S.; Seeger, R.; Pople, J.A. Self-Consistent Molecular-Orbital Methods. 20. Basis Set for Correlated Wave-Functions. *J. Chem. Phys.* **1980**, *72*, 650–654.
32. Groom, C.R.; Bruno, I.J.; Lightfoot, M.P.; Ward, S.C. The Cambridge Structural Database. *Acta Crystallogr.* **2016**, *B72*, 171–179. [CrossRef]
33. Spackman, P.R.; Turner, M.J.; McKinnon, J.J.; Wolff, S.K.; Grimwood, D.J.; Jayatilaka, D.; Spackman, M.A. CrystalExplorer: A program for Hirshfeld surface analysis, visualization and quantitative analysis of molecular crystals. *J. Appl. Crystallogr.* **2021**, *54*, 1006–1011. [CrossRef]
34. Guillot, B.; Enrique, E.; Huder, L.; Jelsch, C. MoProViewer: A tool to study proteins from a charge density science perspective. *Acta Crystallogr.* **2014**, *C70*, 279. [CrossRef]

35. Czerny, F.; Döhlert, P.; Weidauer, M.; Irran, E.; Enthaler, S. Synthesis, characterization and application of nickel(II) complexes modified with *N*,*N*′,*N*″-pincer ligands. *Inorg. Chim. Acta* **2015**, *425*, 118–123. [CrossRef]
36. Meyer, K.; Dalebrook, A.F.; Wright, L.J. Selective palladation of a large (32 ring atom) macrocyclic ligand at a bis(*N*-heterocyclic carbene) coordination pocket through transmetallation of the corresponding mercury(II) derivative. *Dalton Trans.* **2012**, *41*, 14059–14067. [CrossRef]
37. Chen, M.S.; Chen, S.S.; Okamura, T.A.; Su, Z.; Ueyama, N. Syntheses and crystal structures of two supramolecular isomers of manganese (II) with 3,5-bis(isonicotinamido) benzoate. *J. Coord. Chem.* **2009**, *62*, 2421–2428. [CrossRef]
38. Ichii, T.; Arikawa, T.; Omoto, K.; Hosono, N.; Sato, H.; Kitagawa, S.; Tanaka, K. Observation of an exotic state of water in the hydrophilic nanospace of porous coordination polymers. *Nat. Chem. Commun.* **2020**, *3*, 16. [CrossRef]
39. Waris, G.; Siddiqi, H.M.; Flörke, U.; Hussain, R.; Butt, M.S. *N*, *N*′-Bis (4-bromophenyl) pyridine-2, 6-dicarboxamide. *Acta Crystallogr.* **2013**, *E69*, o416. [CrossRef]
40. Gallagher, J.F.; Hehir, N.; Mocilac, P.; Violin, C.; O'Connor, B.F.; Aubert, E.; Espinosa, E.; Guillot, B.; Jelsch, C. Probing the Electronic Properties and Interaction Landscapes in a Series of *N*-(Chlorophenyl)pyridinecarboxamides. *Cryst. Growth Des.* **2022**, *22*, 3343–3358. [CrossRef] [PubMed]
41. Ahmed, E.; Karothu, D.P.; Pejov, L.; Commins, P.; Hu, Q.; Naumov, P. From Mechanical Effects to Mechanochemistry: Softening and Depression of the Melting Point of Deformed Plastic Crystals. *J. Am. Chem. Soc.* **2020**, *142*, 11219–11312. [CrossRef] [PubMed]
42. Jelsch, C.; Ejsmont, K.; Huder, L. The enrichment ratio of atomic contacts in crystals, an indicator derived from the Hirshfeld surface analysis. *IUCrJ* **2014**, *1*, 119–128. [CrossRef] [PubMed]
43. Salonen, L.M.; Ellermann, M.; Diederich, F. Aromatic rings in chemical and biological recognition: Energetics and structures. *Angew. Chem. Int. Ed.* **2011**, *50*, 4808–4842. [CrossRef]
44. Jelsch, C.; Soudani, S.; Ben Nasr, C. Likelihood of atom-atom contacts in crystal structures of halogenated organic compounds. *IUCrJ* **2015**, *2*, 327–340. [CrossRef]
45. Jelsch, C.; Bibila Mayaya Bisseyou, Y. Atom interaction propensities of oxygenated chemical functions in crystal packings. *IUCrJ* **2017**, *4*, 158–174. [CrossRef]
46. Metrangolo, P.; Resnati, G. Type II halogen···halogen contacts are halogen bonds. *IUCrJ* **2014**, *1*, 5–7. [CrossRef]
47. Ramasubbu, N.; Parathasarathy, R.; Murray-Rust, P. Angular preferences of intermolecular forces around halogen centers: Preferred directions of approach of electrophiles and nucleophiles around carbon-halogen bond. *J. Am. Chem. Soc.* **1986**, *108*, 4308–4314. [CrossRef]
48. Thalladi, V.R.; Weiss, H.C.; Bläser, D.; Boese, R.; Nangia, A.; Desiraju, G.R. C−H···F Interactions in the Crystal Structures of Some Fluorobenzenes. *J. Am. Chem. Soc.* **1998**, *120*, 8702–8710. [CrossRef]
49. Britton, D. 4,4′-diiodobiphenyl. *Acta Crystallogr.* **2005**, *E61*, o187–o188. [CrossRef]
50. Lemee, M.H.; Toupet, L.; Delugeard, Y.; Messager, J.C.; Cailleau, H. Crystal structure and thermal-motion analysis of 4,4′-difluorobiphenyl. *Acta Crystallogr.* **1987**, *B43*, 466–470. [CrossRef]
51. Chopra, D.; Row, T.G. Evaluation of the interchangeability of C–H and C–F groups: Insights from crystal packing in a series of isomeric fluorinated benzanilides. *CrystEngComm* **2008**, *10*, 54–67. [CrossRef]
52. Okamoto, T.; Reese, C.; Senatore, M.L.; Tang, M.L.; Jiang, Y.; Parkin, S.R.; Bao, Z. 2,9-Dibromopentacene: Synthesis and the role of substituent and symmetry on solid-state order. *Synth. Met.* **2010**, *21*, 2447–2451. [CrossRef]
53. Saraswatula, V.G.; Saha, B.K. The effect of temperature on interhalogen interactions in a series of isostructural organic systems. *New J. Chem.* **2014**, *38*, 897–901. [CrossRef]
54. Ding, X.; Zahid, E.; Unruh, D.K.; Hutchins, K.M. Differences in thermal expansion and motion ability for herringbone and face-to-face π-stacked solids. *IUCrJ* **2022**, *9*, 31–42. [CrossRef] [PubMed]
55. Varadwaj, A.; Varadwaj, P.R.; Marques, H.M.; Yamashita, K. A DFT assessment of some physical properties of iodine-centered halogen bonding and other non-covalent interactions in some experimentally reported crystal geometries. *Phys. Chem. Chem. Phys.* **2018**, *20*, 15316–15329. [CrossRef]
56. Shallangwa, G.A.; Uzairu, A.; Oltunji Ajibola, V.; Abba, H. Computational Study of the Mechanism of the Oxidation of Hydrazine/Hydrazinium Ion by Iodine in the Gas Phase. *Int. J. Comp. Theor. Chem.* **2015**, *3*, 6–18. [CrossRef]
57. Saccone, M.; Terraneo, G.; Pilati, T.; Cavallo, G.; Priimagi, A.; Metrangolo, P.; Resnati, G. Azobenzene-based difunctional halogen-bond donor: Towards the engineering of photoresponsive co-crystals. *Acta Crystallogr.* **2014**, *B70*, 149–156. [CrossRef] [PubMed]
58. Wang, C.; Danovich, D.; Mo, Y.; Shaik, S. On The Nature of the Chemical Bond. *J. Chem. Theory Comput.* **2014**, *10*, 3726–3737. [CrossRef] [PubMed]
59. Kuznetsov, M.L. Relationships between Interaction Energy and Electron Density Properties for Homo Halogen Bonds of the $[(A)_nY–X\cdots X–Z(B)_m]$ Type (X = Cl, Br, I). *Molecules* **2019**, *24*, 2733. [CrossRef] [PubMed]
60. Lumbreras, M.; Protas, J.; Jebbari, S.; Dirksen, G.J.; Schoonman, J. Structure and ionic conductivity of mixed lead halides $PbCl_{2x}Br_{2(1-x)}$. II. *Solid State Ion.* **1986**, *20*, 295–304. [CrossRef]
61. Altawarneh, M.; Marashdeh, A.; Dlugogorski, B.Z. Structures, electronic properties and stability phase diagrams for copper(I/II) bromide surfaces. *Phys. Chem. Chem. Phys.* **2015**, *17*, 9341–9351. [CrossRef] [PubMed]

62. Meng, G.R.; Zhang, J.; Szostak, M. Acyclic Twisted Amides. *Chem. Rev.* **2021**, *21*, 12746–12783. [CrossRef] [PubMed]
63. Cavallo, G.; Metrangolo, P.; Milani, R.; Pilati, T.; Priimagi, A.; Resnati, G.; Terraneo, G. The Halogen Bond. *Chem. Rev.* **2016**, *116*, 2478–2601. [CrossRef]